

# Reverse Leakage Current Transport Mechanisms in Ni/Au Al<sub>0.58</sub>Ga<sub>0.42</sub>N Schottky Type Photodetectors

Guofeng Yang <sup>✉</sup>, Member, IEEE, Yan Gu, Yushen Liu, Feng Xie, Yuhang Li, Xiumei Zhang, Naiyan Lu, and Chun Zhu

**Abstract**—We successfully fabricated the Al<sub>0.58</sub>Ga<sub>0.42</sub>N-based solar-blind ultraviolet (UV) Schottky type photodetectors (PDs). The crystalline quality, morphology and dislocation information of the Al<sub>0.58</sub>Ga<sub>0.42</sub>N epitaxial layer have been obtained by detailed characterizations of high-resolution X-ray diffraction (XRD), atomic force microscopy (AFM) and transmission electron microscope (TEM). In addition, the responsivity of the PD with cutoff wavelength of 260 nm is 0.15 A/W at -5 V and 0.12 A/W at 5 V, respectively. Detailed carrier transport models are explored to analyze the I-V-T characteristics measured between 300 and 425 K, in order to provide more information for analyzing the reverse leakage mechanisms in the Al<sub>0.58</sub>Ga<sub>0.42</sub>N solar-blind PD. It is convincingly demonstrated that thermionic-field emission and Poole–Frenkel emission can accurately describe the low-bias I-V characteristics and the high-bias I-V characteristics, respectively.

**Index Terms**—AlGaN, carrier transport, Schottky type, ultraviolet photodetectors.

## I. INTRODUCTION

A S WELL known, Ultraviolet (UV) photodetectors (PDs) have been rapidly developed due to their potentially significant applications for UV-emitter calibration, secure space-to-space transmission, gas sensing, flame sensors, biological and chemical sensors, and missile warning systems [1]–[7]. Furthermore, AlGaN-based materials and devices have received

Manuscript received April 19, 2021; revised June 20, 2021; accepted June 23, 2021. Date of publication June 25, 2021; date of current version July 26, 2021. This work was supported in part by the National Natural Science Foundation of China under Grant 61974056, in part by the Key Research and Development Program of Jiangsu Province under Grant BE2020756, in part by the Natural Science Foundation of Jiangsu Province under Grant BK20190576, in part by the Science and Technology Development Foundation of Wuxi under Grant N20191002, in part by the Fundamental Research Funds for Central Universities under Grant JUSRP22032, and in part by the Postgraduate Research & Practice Innovation Program of Jiangsu Province under Grant KYCY20\_1769. (Corresponding author: Guofeng Yang.)

Guofeng Yang, Yan Gu, Yuhang Li, Xiumei Zhang, Naiyan Lu, and Chun Zhu are with the School of Science, Jiangsu Provincial Research Center of Light Industrial Optoelectronic Engineering and Technology, Jiangnan University, Wuxi, Jiangsu 214122, China (e-mail: gfyang@jiangnan.edu.cn; 6171203001@stu.jiangnan.edu.cn; 6191203011@stu.jiangnan.edu.cn; xiumezhang@jiangnan.edu.cn; lunaiyan@jiangnan.edu.cn; chunzhu1979@hotmail.com).

Yushen Liu is with the School of Electronic and Information Engineering, Changshu Institute of Technology, Changshu, Jiangsu 215556, China (e-mail: ysliu@cslt.edu.cn).

Feng Xie is with the The 38th Research Institute of China Electronics Technology Group Corporation, Hefei, Anhui 230000, China (e-mail: fxie@foxmail.com).

Digital Object Identifier 10.1109/JPHOT.2021.3092630

extensive attention because of their outstanding optoelectronic properties in the UV wavelength and the tunable forbidden bandwidth in the range of 3.4 eV~6.2 eV through variable Al-content [8]. The solar-blind UV PDs with Al mole fraction more than 40% possesses the unique ability to be sensitive to UV adiation with wavelengths shorter than 280 nm, which can prevent the solar background radiation from deducing detection sensitivity. In recent years, many studies have reported a variety of (Al)GaN-based UV PDs with different structures [9]–[13], such as photoconductive, metal-semiconductor-metal, Schottky barrier, and p-i-n. In particular, the Schottky barrier detector is of considerable interest for the advantages of simple manufacturing process, no p-type doping, high responsivity and high frequency characteristics. Although there were many works on (Al)GaN-based Schottky barrier UV PDs, the solar-blind type was rarely studied owing to numerous difficulties in obtaining high-quality AlGaN epi-layer [1]. In addition, the crystal quality of AlGaN will deteriorate with the increase of Al content, resulting in structural defects such as dislocations which are the main source of reverse leakage current [14], [15] in the AlGaN epi-layer with high Al-content, and would affect the performance of the devices. Therefore, it is necessary to investigative the reverse-bias charge transport mechanisms for Schottky contacts. Many groups [16]–[20] have performed studies on the dominant transport model resulting in leakage current based on direct experimental measurements and observations. Among them, thermionic-field emission (TFE) is defined as the dominant mechanisms describing carrier transport under conditions of reverse bias and intermediate temperature [21], [22], which can well explain the sharp exponential increase in leakage current with reverse bias. On the other hand, some researchers suggested Poole–Frenkel emission (PFE) is the most suitable mechanism for leakage current at temperatures over 250K for Schottky contacts [20], [23]. Thus, a comprehensive understanding of the leakage current transport mechanisms has great importance on providing guiding suggestions for electronic and optoelectronic devices.

In this work, a Ni/Au-Al<sub>0.58</sub>Ga<sub>0.42</sub>N Schottky type solar-blind UV PD was fabricated, and the Al<sub>0.58</sub>Ga<sub>0.42</sub>N epi-layer was grown by metal organic chemical vapor deposition (MOCVD) on sapphire substrate. The crystalline quality of high-Al-composition Al<sub>0.58</sub>Ga<sub>0.42</sub>N epi-layer was characterized by High-resolution X-ray diffraction (XRD), atomic force microscopy (AFM) and transmission electron microscope (TEM). Moreover, the fabricated PD device exhibited outstanding

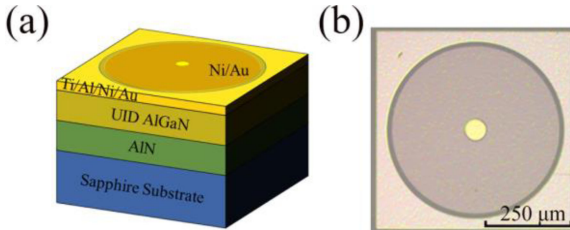


Fig. 1. (a) Three-dimensional structural diagram of AlGaN-based Schottky-type PD. (b) The top-view optical micrograph of the fabricated Schottky-type solar-blind UV PD with a Schottky contact of  $500\ \mu\text{m}$  in diameter.

performances. The temperature-related current-voltage curves were measured to systematically investigate the reverse leakage current carrier transport mechanisms of the  $\text{Al}_{0.58}\text{Ga}_{0.42}\text{N}$  solar-blind PDs.

## II. EXPERIMENTAL DETAILS

The AlGaN-based Schottky-type PD structural diagrams are shown in the Fig. 1. The epitaxial layers shown in Fig. 1(a) consisting of a 1-μm unintentionally doped (UID)  $\text{Al}_{0.58}\text{Ga}_{0.42}\text{N}$  active layer on top of a 1-μm AlN buffer layer were grown on a c-plane sapphire substrate by MOVCD system. Fig. 1(b) displays the top-view photograph of electrodes consisting of the circular Schottky dot with a diameter of 500 μm radially separated from the ohmic metal by 14 μm. The Ohmic contact was fabricated by depositing Ti (10 nm)/Al (70 nm)/Ni (10 nm)/Au (100 nm) metal stack using e-beam evaporation and performing a rapid thermal annealing process under  $\text{N}_2$  environment at 750 °C for about 60 s. The semitransparent Schottky contacts were formed based on Ni (40 nm)/Au (100 nm) metal stack on the surface of  $\text{Al}_{0.58}\text{Ga}_{0.42}\text{N}$  active layer using e-beam evaporation and patterned by standard photolithography and lift-off technologies.

The characterization and morphology of the  $\text{Al}_{0.58}\text{Ga}_{0.42}\text{N}$  epi-layer were carried out by high-resolution X-ray diffraction (XRD) and Atomic force microscopy (AFM). The transmission electron microscope (TEM) measurements were employed to analyze the crystal information and estimate dislocation densities. The I-V curves at room- and high-temperature were achieved by probe station with a Keithley 4200 semiconductor parameter analyzer. Besides, a 500 W xenon lamp was used to measure the spectral responsivity curves of solar-blind UV PDs.

## III. RESULTS AND DISCUSSION

The characterization methods such as XRD, AFM and TEM were used to describe the crystal structure and crystalline quality of the MOCVD-grown AlGaN. The  $\omega/\theta$  scan rocking curves in Fig. 2(a) display the values of full-width at half-maximum (FWHM) for (0002) and (10-12) planes of AlGaN with high Al-content are 330 arcsec and 644 arcsec, respectively, indicating a high crystalline quality of the AlGaN active layer. Besides, it is obvious from Fig. 2(b) that two diffraction peaks represent the epi-layers of AlGaN and AlN, respectively. As shown in Fig. 2(c), the AFM image over a typical area of  $5 \times 5\ \mu\text{m}^2$  exhibits the surface morphology of AlGaN with a root-mean-square (RMS) surface roughness value of 1.125 nm. Fig. 2(d)

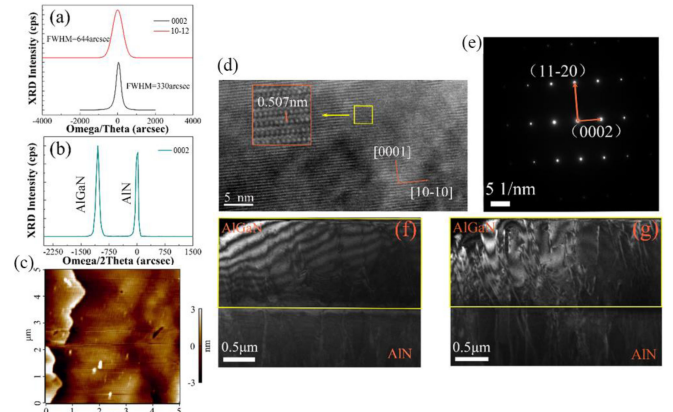


Fig. 2. XRD spectrums of the epi-layer: (a)  $\omega/\theta$  rocking curves of the (0002) and (10-12) planes for AlGaN active layer and (b)  $\omega/2\theta$  scan of the (0002) plane. (c) AFM image of  $\text{Al}_{0.58}\text{Ga}_{0.42}\text{N}$  epi-layer with  $5\ \mu\text{m} \times 5\ \mu\text{m}$ . TEM patterns: (d) HRTEM image of  $\text{Al}_{0.58}\text{Ga}_{0.42}\text{N}$  epi-layer (the red square in the inset shows magnification of the yellow frame area), (e) SAED image of  $\text{Al}_{0.58}\text{Ga}_{0.42}\text{N}$ , (f) and (g) dark-field cross-sectional TEM micrographs for the AlN/ $\text{Al}_{0.58}\text{Ga}_{0.42}\text{N}$  epitaxial structure.

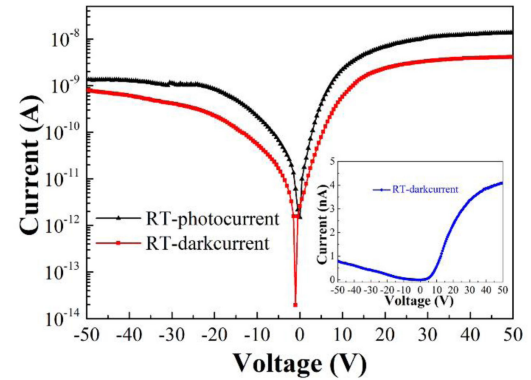


Fig. 3. The current-voltage (I-V) curves without light illumination and with 280-nm light illumination under room-temperature. The inset shows the linear I-V characteristic in dark.

and (e) show the TEM patterns which are used to characterize the crystal structure of AlGaN in detail. The [0001] and [10-10] crystal orientations are marked in the high-resolution TEM (HRTEM) image of AlGaN epi-layer shown in Fig. 2(d). In addition, from the insert of Fig. 2(d), the Al content of 0.58 has been obtained by calibrating the c-direction lattice constant of 0.507 nm, which agrees with the spacing of the (001) plane of the  $\text{Al}_{0.58}\text{Ga}_{0.42}\text{N}$  ( $d(0001) \approx 5.067\text{\AA}$ ). The single crystalline wurtzite nature of the  $\text{Al}_{0.58}\text{Ga}_{0.42}\text{N}$  has been confirmed according to the spotted selected area electron diffraction (SEAD) pattern displayed in Fig. 2(e), and [11]-[20] and [0001] crystal planes can be calibrated. The dark-field cross-sectional TEM micrographs of AlGaN/AlN displayed in Fig. 2(f) and (g) are employed to analyze the defects of epitaxially grown AlGaN. It is clear that the distribution of the dislocation lines exists in the AlGaN epi-layer. The dislocation density estimated by counting the number of dislocation lines in the cross-sectional TEM images corresponds to the density of screw and edge dislocations [23], [24]. Fig. 2(f) shows the morphology of screw dislocation whose density is estimated to be about

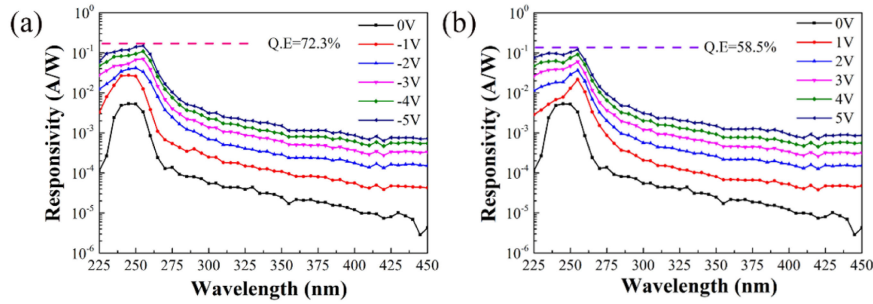


Fig. 4. Spectral response of the Schottky type PD under (a) reverse and (b) forward bias voltages at room temperature.

$3.48 \times 10^8 \text{ cm}^{-2}$  under the diffraction vectors  $\mathbf{g} = [0002]$ . On the other hand, Fig. 2(f) shows the morphology of edge dislocation, the density of which is estimated to be about  $1.15 \times 10^9 \text{ cm}^{-2}$  under the diffraction vectors  $\mathbf{g} = [11]-[20]$ .

Fig. 3 shows the current-voltage (I-V) characteristic of the  $\text{Al}_{0.58}\text{Ga}_{0.42}\text{N}$ -based solar-blind Schottky-type PD without light illumination and with 280-nm light illumination at room-temperature. The fabricated PD exhibits a dark current of only 0.78 nA even at the reverse bias of -50 V, which is attributed to the low screw dislocation density of the  $\text{Al}_{0.58}\text{Ga}_{0.42}\text{N}$  active layer. Simultaneously, the dark current is 4.1 nA at a forward voltage of 50 V. In addition, the photocurrent of 14 nA under forward voltage (50 V) and 1.33 nA under reverse bias voltage (-50 V) are obtained under 280nm-light illumination. It is obvious from the inset of Fig. 3 that the dark current of the device at the forward voltage is much larger than that under the reverse voltage, demonstrating that the device exhibits rectification characteristics and compound Schottky barrier diode characteristics.

Fig. 4(a) and (b) show the bias-dependent spectral response curves at reverse and forward bias voltage calibrated by standard Si-based PD. The photoresponsivity peak is 0.15A/W at voltage of -5V with the quantum efficiency reaching 72%. While for the forward bias voltage, photoresponsivity peak of 0.12A/W can be obtained with the quantum efficiency of 58.5% at 5V. It is evident that the peak of the response curves under reverse and forward bias voltage approximately appear at 255 nm excepting bias of 0V, -1V, -2V (250nm) due to the electric field and the experimental environment. Besides, it begins to cut off at 260 nm, which is in good agreement with the bandgap wavelength of  $\text{Al}_{0.58}\text{Ga}_{0.42}\text{N}$  of 259nm estimated based on the band gap energy given by

$$E_g(\text{Al}_x\text{Ga}_{1-x}\text{N}) = 3.4(1-x) + 6.2x - x(1-x) \quad (1)$$

Fig. 5 shows the dark current depends on both voltage and temperature ranging from 300 to 425K. It can be seen that the dark current increases as temperature increases. Since the results show a strong dependence on bias at all temperatures, it can be excluded out that carrier emission over the Schottky barrier formed at the metal-semiconductor interface contributes to the transport mechanism. In addition, I-V-T curves demonstrate that the reverse dark current has a sharp exponential dependence on voltage in the low-bias regime, and then reveals a weak dependence on high field. As a result, it is essential to discuss

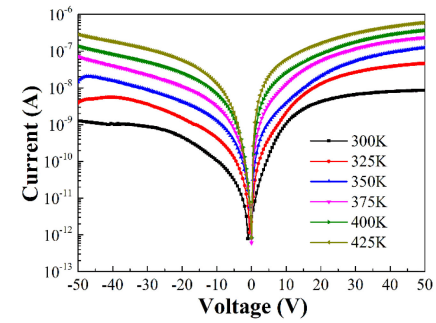


Fig. 5. High-temperature dependent I-V characteristics of  $\text{Al}_{0.58}\text{Ga}_{0.42}\text{N}$ -based Schottky type PD at different temperatures.

possible electrons transport models based on the measured I-V-T characteristics in the following paragraphs.

The TFE model for tunneling transport mechanism can be employed to analyze a sharp exponential dependence of the leakage current on reverse voltage under low field. The relationship between current and reverse bias based on TFE model can be described by [21]

$$I_{\text{TFE}} = I_s e^{\left(-\frac{qV_R}{\varepsilon'}\right)} \quad (2)$$

where  $I_s$  is the saturation current,  $V_R$  is the reverse voltage, and  $\varepsilon'$  is energy parameter associated with temperature, which can be given by

$$\varepsilon' = \frac{E_{00}}{\left[\frac{E_{00}}{kT} - \tanh\left(\frac{E_{00}}{kT}\right)\right]} \quad (3)$$

$$E_{00} = \frac{\hbar}{2} \sqrt{\frac{N_D}{m * \varepsilon_0 \varepsilon_s}} \quad (4)$$

in which  $E_{00}$  is an energy parameter,  $k$  is Boltzmann's constant,  $T$  is the temperature,  $\hbar$  is reduced Planck's constant,  $m*$  is effective electron mass,  $N_D$  is donor density, and  $\varepsilon_s \varepsilon_0$  is dielectric constant of the semiconductor. Fig. 6(a) exhibits the comparison results between linear fitting curves using (1) and experimental data of  $\ln(I)-V$  in a temperature range from 300 to 425K, indicating the validity of this potential mechanism for the  $\text{Al}_{0.58}\text{Ga}_{0.42}\text{N}$ -based Schottky type PD. Moreover, Fig. 6(b) displays variations of energy parameter  $\varepsilon'$  and  $E_{00}$  as a function of temperature by extracting the slopes of the fitting lines and calculating (3). The specific values of  $\varepsilon'$ ,  $E_{00}$

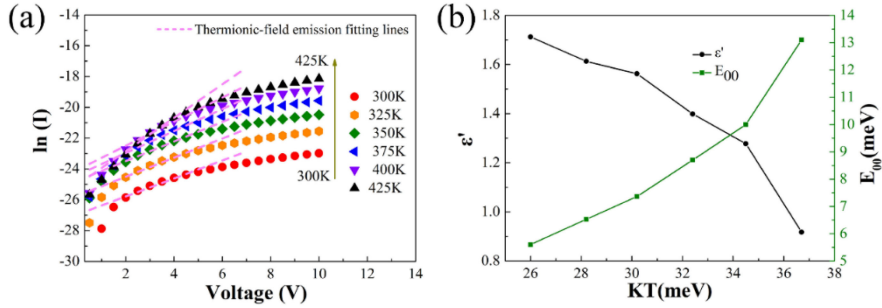


Fig. 6. (a) The fitting results for  $\ln(I)$ -V characteristics using TFE as transport model. (b) The values of  $\epsilon'$  and  $E_{00}$  extracted from the slope of the fitting curves.

TABLE I  
FITTING PARAMETERS BASED ON TFE

| Temperature (K) | $\epsilon'$ | kT (meV) | $E_{00}$ | $kT/E_{00}$ |
|-----------------|-------------|----------|----------|-------------|
| 300K            | 1.71        | 26       | 5.6      | 4.6         |
| 325K            | 1.61        | 28.2     | 6.53     | 4.3         |
| 350K            | 1.56        | 30.2     | 7.36     | 4.1         |
| 375K            | 1.39        | 32.4     | 8.7      | 3.7         |
| 400K            | 1.28        | 34.5     | 9.98     | 3.45        |
| 425K            | 0.91        | 36.7     | 13.1     | 2.8         |

and thermal energy  $k_T$  can be obtained from Table I at each temperature. As suggested in the literatures [22], [26], the ratio of  $E_{00}$  to  $k_T$  can examine which of TE, FE and TFE is the main transport mechanism. That is, field emission will dominate when  $kT/E_{00} \ll 1$ , conversely, thermionic emission will occur when  $kT/E_{00} \gg 1$ . If  $kT/E_{00} \approx 1$ , thermionic-field emission dominates charge transport. Thus, according to the values of  $kT/E_{00}$  shown in Table I, which reveals  $E_{00}$  is close to  $kT$  at each temperature, it is confirmed that TFE transport model dominates tunneling of carrier from metal Fermi level into  $\text{Al}_{0.58}\text{Ga}_{0.42}\text{N}$  conduction band at low reverse-bias.

Given a relatively weak dependence of reverse leakage current on the high applied bias, linear variety of  $\ln(I_{PF}/E)$  with respect to  $\sqrt{E}$  can be observed according to PFE as the possible transport mechanism. The leakage current transport due to PFE can be described as [27]

$$I_{PF} = AE \exp \left[ -\frac{q(\phi_t - \sqrt{qE/\pi\varepsilon_s\varepsilon_0})}{kT} \right] \quad (5)$$

and  $\ln(I_{PF}/E)$  vs  $\sqrt{E}$  can be written by

$$\begin{aligned} \ln(I_{PF}/E) &= \ln(A) - \frac{q}{kT}\phi_t + \frac{q}{kT}\sqrt{\frac{qE}{\pi\varepsilon_s\varepsilon_0}} \\ &\equiv a(T) + b(T)\sqrt{E} \end{aligned} \quad (6)$$

$$a(T) = -\frac{q}{kT}\phi_t + \ln(A) \quad (7)$$

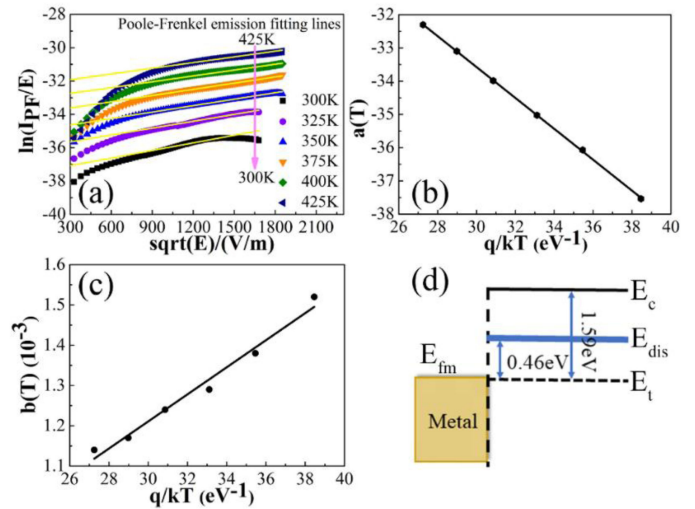


Fig. 7. (a) The linear fitting results for  $\ln(I_{PF}/E)$ - $\sqrt{E}$  characteristics using PFE transport model. (b) Intercepts  $a(T)$  vary with respect to  $q/kT$ . (c) Slopes  $b(T)$  vary with respect to  $q/kT$ . (d) Energy band diagram with  $E_t$  located 0.46eV below dislocation-related trap state  $E_{dis}$ .

$$b(T) = \frac{q}{kT} \sqrt{\frac{q}{\pi\varepsilon_s\varepsilon_0}} \quad (8)$$

Here,  $kT$  is thermal energy,  $\varepsilon_0$  is the permittivity of free space,  $\varepsilon_s$  is the relative dielectric permittivity at high frequency, and  $\Phi_t$  is the barrier for electron emission from the trap state. It is evident from Fig. 7(a) that the calculated  $\ln(I_{PF}/E)$  vary linearly with  $\sqrt{E}$ , indicating that the current can be well described by (5) and (6), thus confirming the potential of PFE as a transport mechanism. Moreover, the values of physical parameters  $\Phi_t$  and  $\varepsilon_s$  can be obtained by extracting the slope from (7) and (8). From the linear fitting results shown in Fig. 7(a) and (b),  $\Phi_t$  is estimated about 0.46 eV by the slope of  $a(T)$  vs  $q/kT$ , and  $\varepsilon_s^{\text{Al}0.58\text{Ga}0.4\text{N}}$  is estimated about 5.14 by the slope of  $b(T)$  vs  $q/kT$ . Furthermore, the value of 5.14 obtained for  $\varepsilon_s^{\text{Al}0.58\text{Ga}0.4\text{N}}$  is reasonable based on the values of 5.35 for  $\varepsilon_s^{\text{GaN}}$  and 4.77 for  $\varepsilon_s^{\text{AlN}}$  reported in the literatures [28], [29], verifying the dominance of PFE as a carrier transport mechanism. Fig. 7(d) shows the energy band diagram where the trap level should near the metal Fermi level, indicating that the dominant factor for the leakage current is likely that carriers undergo PFE from a trap state into conductive dislocation-related continuum of states.

However, the assumption that the trap level is positioned 0.46 eV below the Al<sub>0.58</sub>Ga<sub>0.42</sub>N conduction band can be ruled out, since in which the direct thermionic emission rather than PFE via a trap state will govern charge transport base on the Ni/Al<sub>0.58</sub>Ga<sub>0.42</sub>N Schottky barrier height of 1.59 eV [30]. Therefore, it can be concluded that the Frenkel-Poole emission model can accurately describe the current transmission process varying with temperature and electric field by reasonable physical parameters.

#### IV. CONCLUSION

In summary, the solar-blind Al<sub>0.58</sub>Ga<sub>0.42</sub>N-based Schottky UV PDs have been successfully fabricated. The Al<sub>0.58</sub>Ga<sub>0.42</sub>N active epi-layer exhibits an ideal morphology with RMS of 1.125 nm, and its FWHMs are 330 arcsec and 644 arcsec for (002) and (102) planes, respectively. The single crystal wurtzite nature and estimated dislocation density are obtained by HRTEM. Moreover, the highest peak responsivity of fabricated solar-blind PD reaches 0.15A/W at -5 V and 0.12A/W at 5V. Additionally, two describing reverse leakage current models (TFE and PFE) are purposed to explain the experimental I-V-T characteristics. For low bias voltage, the leakage process is that electrons tunnel from metal into the Al<sub>0.58</sub>Ga<sub>0.42</sub>N conduction band through thermal field emission according to  $kT/E_{00} \approx 1$ . For high bias voltage, the agreement between the fitting I-V curves and the experimental results suggests that carrier transport from a trap state into dislocation-related continuum of states by PFE.

#### REFERENCES

- [1] D. H. Wang *et al.*, "Pt/AlGaN nanoarchitecture: Toward high responsivity, self powered ultraviolet-sensitive photodetection," *Nano Lett.*, vol. 20, no. 1, pp. 120–129, 2021.
- [2] D. Y. Guo, Q. X. Guo, Z. W. Chen, Z. P. Wu, P. G. Li, and W. H. Tang, "Review of Ga<sub>2</sub>O<sub>3</sub>-based optoelectronic devices," *Mater. Today Phys.*, vol. 11, 2019, Art. no. 100157.
- [3] D. H. Wang *et al.*, "Highly uniform, self-assembled AlGaN nanowires for self-powered solar-blind photodetector with fast-response speed and high responsivity," *Adv. Opt. Mater.*, vol. 9, no. 4, 2021, Art. no. 2000893.
- [4] D. Y. Guo *et al.*, "Self-powered solar-blind photodetectors based on alpha/beta phase junction of Ga<sub>2</sub>O<sub>3</sub>," *Phys. Rev. Appl.*, vol. 13, no. 2, 2020, Art. no. 024051.
- [5] Z. J. Ren *et al.*, "Band engineering of III-nitride-based deep-ultraviolet light-emitting diodes: A review," *J. Phys. D-App. Phys.*, vol. 53, no. 7, 2020, Art. no. 073002.
- [6] H. Zhang *et al.*, "Compositionally graded III-nitride alloys: Building blocks for efficient ultraviolet optoelectronics and power electronics," *Rep. Prog. Phys.*, vol. 84, no. 4, 2021, Art. no. 044401.
- [7] C. Huang, H. Zhang, and H. Sun, "Ultraviolet optoelectronic devices based on AlGaN-SiC platform: Towards monolithic photonics integration system," *Nano Energy*, vol. 77, 2020, Art. no. 105149.
- [8] F. Xie *et al.*, "Large-area solar-blind algan-based MSM photodetectors with ultra-low dark current," *Electron. Lett.*, vol. 47, no. 16, pp. 930–931, 2011.
- [9] M. Brendel, M. Helbling, A. Knigge, F. Brunner, and M. Weyers, "Solar-blind AlGaN MSM photodetectors with 24% external quantum efficiency at 0 V," *Electron. Lett.*, vol. 51, no. 20, pp. 1598–1599, 2015.
- [10] J. A. Garrido, E. Monroy, I. Izpura, and E. Munoz, "Photoconductive gain modelling of GaN photoconductors," *Semicond. Sci. Technol.*, vol. 13, no. 6, pp. 563–568, 1998.
- [11] R. McClintock *et al.*, "High quantum efficiency AlGaN solar-blind p-i-n photodiodes," *Appl. Phys. Lett.*, vol. 84, no. 8, pp. 1248–1250, 2004.
- [12] A. Osinsky *et al.*, "Visible-blind GaN Schottky barrier detectors grown on si(111)," *Appl. Phys. Lett.*, vol. 72, no. 5, pp. 551–553, 1998.
- [13] F. Xie *et al.*, "Bias-selective dual-operation-mode ultraviolet Schottky-barrier photodetectors fabricated on high-resistivity homoepitaxial GaN," *IEEE Photon. Technol. Lett.*, vol. 24, no. 24, pp. 2203–2205, 2012.
- [14] D. B. Li *et al.*, "Influence of threading dislocations on GaN-based metal-semiconductor-metal ultraviolet photodetectors," *Appl. Phys. Lett.*, vol. 98, no. 1, 2011, Art. no. 011108.
- [15] S. Walde, M. Brendel, U. Zeimer, F. Brunner, S. Hagedorn, and M. Weyers, "Impact of open-core threading dislocations on the performance of AlGaN metal-semiconductor-metal photodetectors," *J. Appl. Phys.*, vol. 123, no. 16, 2018, Art. no. 161551.
- [16] L. L. Chen *et al.*, "Charge transport in vertical GaN Schottky barrier diodes: A refined physical model for conductive dislocations," *IEEE Trans. Electron Devices*, vol. 67, no. 3, pp. 841–846, Mar. 2020.
- [17] T.-C. Nam, J.-S. Jang, and T.-Y. Seong, "Carrier transport mechanism of strained AlGaN/GaN schottky contacts," *Curr. Appl. Phys.*, vol. 12, no. 4, pp. 1081–1083 2012.
- [18] S. Oyama, T. Hashizume, and H. Hasegawa, "Mechanism of current leakage through metal/n-GaN interfaces," *Appl. Surf. Sci.*, vol. 190, no. 1-4, pp. 322–325, 2002.
- [19] S. Rathkanthiwar, A. Kaira, R. Muralidharan, D. N. Nath, and S. Raghavan, "Analysis of screw dislocation mediated dark current in Al<sub>0.50</sub>Ga<sub>0.50</sub>N solar-blind metal-semiconductor-metal photodetectors," *J. Cryst. Growth*, vol. 498, pp. 35–42, 2018.
- [20] H. Zhang, E. J. Miller, and E. T. Yu, "Analysis of leakage current mechanisms in Schottky contacts to GaN and Al<sub>0.25</sub>Ga<sub>0.75</sub>N/GaN grown by molecular-beam epitaxy," *J. Appl. Phys.*, vol. 99, no. 2, 2006, Art. no. 023703.
- [21] F. A. Padovani and R. Stratton, "Field and thermionic-field emission in schottky barriers," *Solid-State Electron.*, vol. 9, pp. 695–707, 1966.
- [22] S. Rathkanthiwar *et al.*, "Gain mechanism and carrier transport in high responsivity algan-based solar blind metal semiconductor metal photodetectors," *J. Appl. Phys.*, vol. 121, no. 16, 2017, Art. no. 164502.
- [23] T. Hino, S. Tomiya, T. Miyajima, K. Yanashima, S. Hashimoto, and M. Ikeda, "Characterization of threading dislocations in GaN epitaxial layers," *Appl. Phys. Lett.*, vol. 76, no. 23, pp. 3421–3423, 2000.
- [24] J. Peščík, R. Kužel, A. Dronhofer, and G. Eggeler, "The evolution of dislocation density during heat treatment and creep of tempered martensite ferritic steels," *Acta Materialia*, vol. 51, no. 16, pp. 4847–4862, 2003.
- [25] E. Arslan, S. Butun, and E. Ozbay, "Leakage current by Frenkel-Poole emission in Ni/Au Schottky contacts on Al<sub>0.83</sub>In<sub>0.17</sub>N/AlN/GaN heterostructures," *Appl. Phys. Lett.*, vol. 94, no. 14, 2009, Art. no. 142106.
- [26] C. R. Crowell and V. L. Rideout, "Normalized thermionic-field (T-F) emission in metal-semiconductor (Schottky) barriers," *Solid-State Electron.*, vol. 12, no. 2, pp. 89–105, 1969.
- [27] K. H. Lee, P. C. Chang, S. J. Chang, and S. L. Wu, "GaN-based schottky barrier ultraviolet photodetector with a 5-pair AlGaN-GaN intermediate layer," *Phys. Status Solidi A-App. Mat.*, vol. 209, no. 3, pp. 579–584, 2012.
- [28] A. S. Barker and M. Ilegems, "Infrared lattice vibrations and free-electron dispersion in GaN," *Phys. Rev. B*, vol. 7, no. 2, pp. 743–750, 1973.
- [29] V. W. L. Chin, T. L. Tansley, and T. Osotchan, "Electron mobilities in gallium, indium, and aluminum nitrides," *J. Appl. Phys.*, vol. 75, pp. 7365–7372, 1994.
- [30] O. Ambacher *et al.*, "Pyroelectric properties of Al(In)GaN/GaN hetero- and quantum well structures," *J. Phys.-Condes. Matter*, vol. 14, no. 13, pp. 3399–3434, 2002.